CHAPTER II

MATERIAL PROPERTIES OF CIS-BASED THIN FILMS AND SOLAR CELLS

This chapter will start with a review of the material properties of the ternary compounds that were utilized for photovoltaic devices. The physical principle underlying the solar cell will be briefly described. The common solar cell parameters used to characterize the cell performance will be presented.

2.1 Material Properties of CIS-Based Thin Films

2.1.1 The Cu-In-Se Material System

The thermochemistry of the Cu-In-Se ternary material system has been intensely studied. The Cu_2Se-In_2Se_3 section of the Cu-In-Se phase diagram was first published in the pseudobinary form by Palatnik and Rogacheva in 1966. Various values for the critical point temperature and compositions have been reported. These studies have been assessed by Chang *et al.* [21] resulting in the phase diagram for the pseudobinary section as shown in Fig. 2.1.

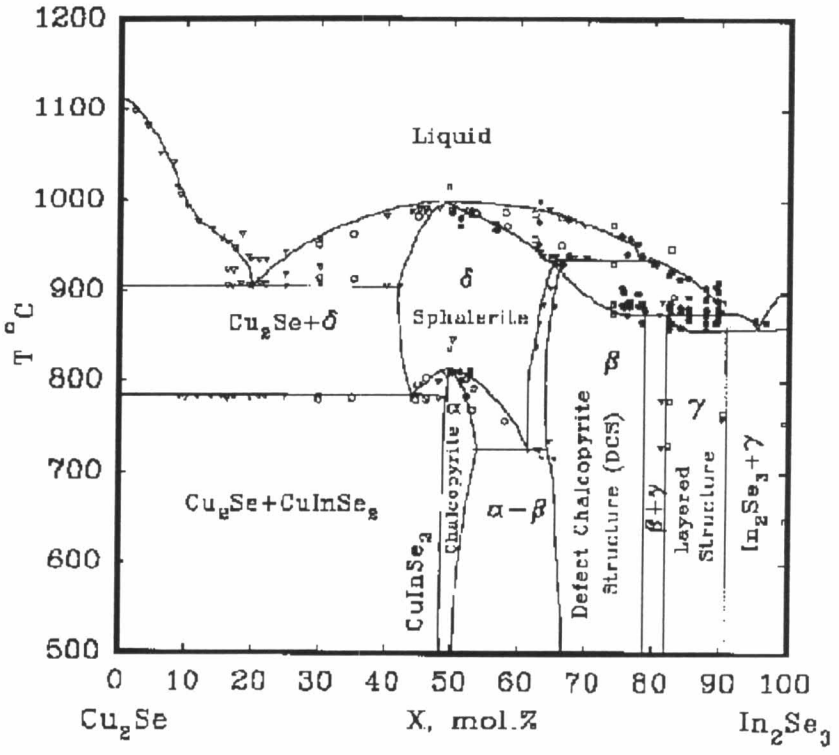

Figure 2.1: Phase diagram along the Cu_2Se-In_2Se_3 pseudobinary section of the Cu-In-Se material system [21].

The phase diagram indicates that the α and δ phases belong to the chalcopyrite and sphalerite crystal structures, respectively. The β phase is referred to be a defect chalcopyrite structure of solid solutions within a composition range bounded by $Cu_2In_4Se_7$ and $CuIn_5Se_8$. The $CuIn_5Se_8$ compound is tentatively included in the γ phase with a layered structure.

The most important conclusions are that the chalcopyrite single phase $CuInSe_2$ extends from a stoichiometric composition of 50 mol% of In_2Se_3 to In-rich composition of about 55 mol% of In_2Se_3. The corresponding Cu/In atomic ratios for this single phase lies between 1.0 and 0.82. In the case of the atomic ratios of Cu/In are greater than 1.0, the materials are expected to contain the secondary phase of Cu_2Se and for contrary cases (Cu/In atomic ratio less

than 1.0) the materials are expected to contain secondary phases of $Cu_2In_4Se_7$ and $CuIn_3Se_5$. Although it is known that the growth from the Cu-rich side of the Cu_2Se-In_2Se_3 pseudobinary phase diagram leads to large grain sizes and good structural property. It has also been shown that the growth of Cu-rich film leads to a formation of the $Cu_{2-x}Se$ phase at the grain boundaries. Most of the high efficiencies CIS thin film solar cells have been fabricated starting from Cu-rich and ending at the slightly Cu-poor composition.

2.1.2 Crystal Structure of $CuInSe_2$

The $CuInSe_2$ crystal belongs to the I-III-VI_2 ternary compounds which crystallize in the chalcopyrite structure and have the space group symmetry $I\bar{4}2d$ [22]. They are the simplest structure analogs of II-VI, ZnSe, zincblende compound. Therefore their crystal structures are expected to be very similar.

The zincblende structure consists of two interpenetrating face centered cubic sublattices. The two sublattices are displaced by one quarter of a body diagonal, each sublattice having only one type of atoms. These may be considered as a cation (Zn) sublattice and an anion (Se) sublattice. In each $CuInSe_2$ compound, the anion sublattice is occupied by the Se atoms, while the cation sublattice is shared by the Cu and In atoms. If the Cu and In atoms are randomly distributed in the sublattice the structure of the compound remains zincblende. However, if they are ordered as shown in Fig. 2.2(a), the structure of the compound is chalcopyrite. Hence each cation Cu and In in the $CuInSe_2$ compound has four Se anions as nearest neighbors, and each anion Se has two Cu and two In cations as nearest neighbors, (see Fig. 2.2(b)). Because of the difference in the strengths between the Cu-Se and In-Se bonds, there are

additional noncubic aspects of chalcopyrite structure, i.e., 1) a doubling of the unit cell in the z-direction resulting from an ordering of the two cations, 2) a compression of the crystal lattice along the c-axis as indicated by a tetragonal distortion ($2-\frac{c}{a}$) and 3) anionic displacements of the anion sites away from the cubic (1/4, 1/4, 1/4) to the tetragonal (0, 1/4, 1/8) position and symmetrically related positions due to the unequal bond lengths between Cu-Se and In-Se ions.

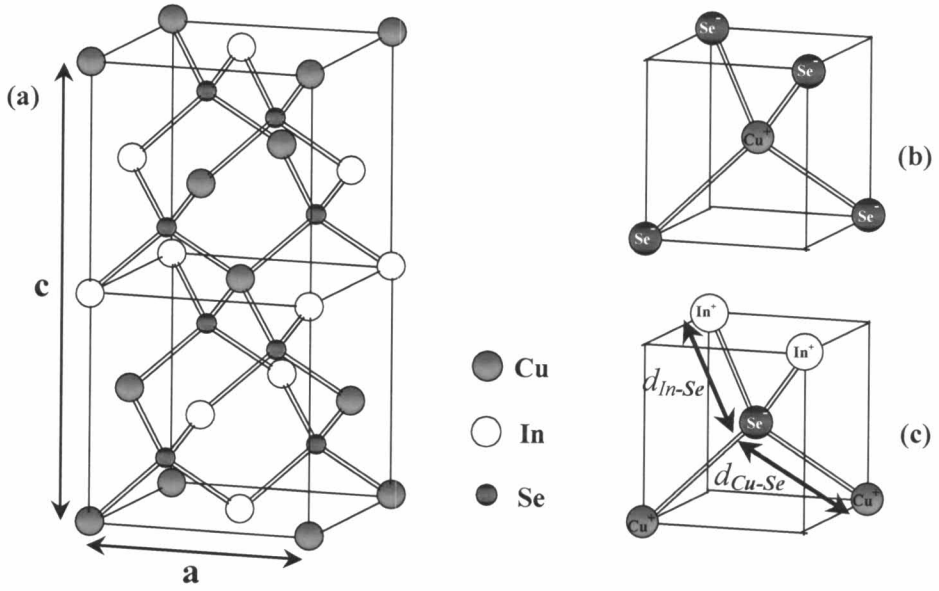

Figure 2.2: Schematic representation of $CuInSe_2$ chalcopyrite structure [23]
(a) conventional unit cell, (b) cation-centered first coordinate shell
(c) anion-centered first coordinate shell showing bond lengths $d_{Cu\text{-}Se}$ and $d_{In\text{-}Se}$.

The $CuIn_{1-x}Ga_xSe_2$ alloy system has also been reported to have a complete solid solubility and mixed crystal formation [24]. The lattice constants a and c/2 of this system is shown in Fig. 2.3. Their band gap energies varies between 1.0 - 2.4 eV and their absorption coefficients are in the order of

10^5 cm^{-1} [8, 24, 25, 26]. So they are good candidate materials for solar cell applications.

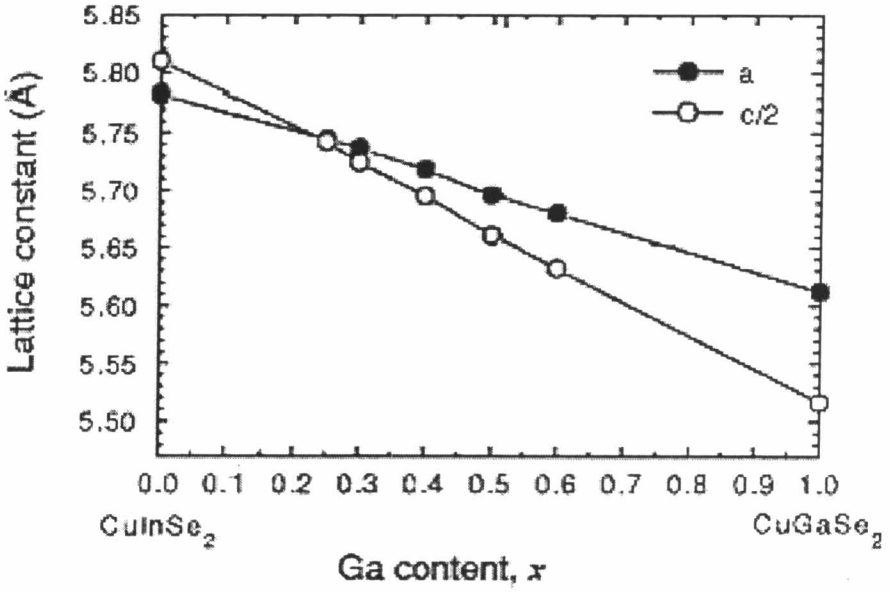

Figure 2.3: Lattice constants a and c/2 of the $CuInSe_2$-$CuGaSe_2$ alloy system [26].

2.1.3 Defect of $CuInSe_2$

Generally, the defect chemistry model of CIS was proposed for its nearly stoichiometric compound by Rincon *et al.* [27]. The deviation of its actual composition from the ideal formula can be described by two parameters, the molecularity deviation Δm and the stoichiometry deviation Δs. These parameters have been defined as [27, 28]

$$\Delta m = \frac{[Cu]}{[In]} - 1 \quad \text{; molecularity deviation} \quad , \qquad (2.1)$$

$$\Delta s = \frac{2[Se]}{[Cu] + 3[In]} - 1 \quad \text{; stoichiometry deviation} \quad , \qquad (2.2)$$

where [Cu], [In] and [Se] are the total atomic concentrations of Cu, In and Se respectively in $CuInSe_2$ and [Cu]+[In]+[Se]=1. In the case of nominal $CuInSe_2$, an excess of Cu_2Se gives $\Delta m > 0$, and an excess of In_2Se_3 gives $\Delta m < 0$. Δs determines whether there is an excess ($\Delta s > 0$) or deficiency ($\Delta s < 0$) of selenium. These two parameters give us the different conditions for all possible major defect pairs which can be present under In-rich condition ($\Delta m < 0$) as shown in Table 2.1. The defect formation energies in $CuInSe_2$ are also given in Table 2.2. The data shows that the Cu vacancy defect (V_{Cu}) and the In-on-Cu antisite (In_{Cu}) are the dominant defects in Cu-poor $CuInSe_2$, which need a smaller energy of formation. The V_{Cu} and In_{Cu} can be attributed to a defect pair ($2V_{Cu}+In_{Cu}$) called the neutral defect complex (NDC). This result is in agreement with those of Zhang *et al.* [29], who proposed that the pairing of defects can change the electrical property in the sample. For example, an isolated V_{Cu} is a shallow acceptor, while an isolated In_{Cu} is a deep donor, but a defect pair based on $2V_{Cu}$ and In_{Cu} is electrically inactive. Therefore, they attributed very efficient self-doping ability of $CuInSe_2$ to the exceptionally low formation energy of Cu vacancies (V_{Cu}) and to the existence of a shallow Cu vacancy acceptor level.

Table 2.1: Majority defect pairs in $CuInSe_2$ under the condition $\Delta m < 0$ [27].

Majority defect pair		Stoichiometry deviation
Acceptor	Donor	(Δs)
V_{Cu}	In_{Cu}	< 0
V_{Cu}	V_{Se}	< 0
V_{Cu}	In_i	> 0
Se_i	In_{Se}	> 0
Se_i	In_i	> 0

Table 2.2: Formation energies of intrinsic defects in $CuInSe_2$ [27].

Type of defects		Formation energy (eV)
Vacancies	V_{Se}	2.4
	V_{Cu}	2.6
	V_{In}	2.8
Interstitials	Cu_i	4.4
	In_i	9.1
	Se_i	22.4
Antisites	In_{Cu}	1.4
	Cu_{In}	1.5
	In_{Se}	5.0
	Se_{In}	5.5
	Se_{Cu}	7.5
	Cu_{Se}	7.5

2.2 Physical Principle of the Solar Cell

2.2.1 Solar Spectrum

The spectral irradiation density of the sunlight (power per unit area and per unit wavelength) and the distribution approximation of a black body radiation at 5800 K can be shown in Fig. 2.4.

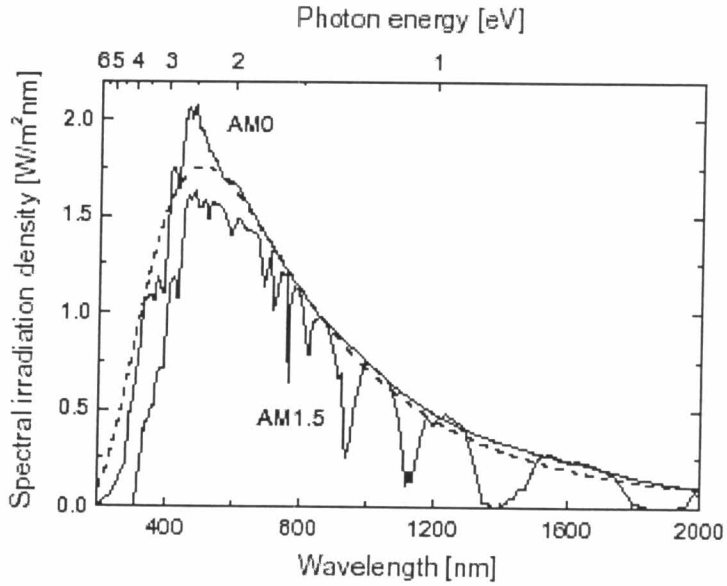

Figure 2.4: Spectral energy distribution for space (AM0), Central Europe (AM1.5), and the theoretical curve for a black body at about 5800 K (dashed line). The upper scale in the figure shows the energy of the photons corresponding to the wavelength in the lower scale [30].

The deviation at certain wavelength is due to absorption effects in Earth's atmosphere. The path length of the radiation through Earth's atmosphere can be described in terms of "air mass" (AM). AM0 corresponds to

the irradiation of the sun without any absorption in the atmosphere. AM1 corresponds to the irradiation at the equator and AM1.5 is the irradiation in Central Europe with a total power density of 0.844 kW/m^2. This number is being adopted as a standard.

Theoretical calculations of efficiency for different sun spectra are shown in Fig. 2.5 [31]. It indicates that the optimal band gap of the absorber layer occurs between 1.4 and 1.6 eV. The near-optimal efficiency (29%) for AM1.5 with 1 sun (C = 1) irradiation occurs at GaAs (1.4 eV), whereas the peak efficiency for silicon (1.1 eV) of about 26% is lower than optimum but still relatively high. Moreover, the curve of efficiency for AM1.5 with 1000 suns (C = 1000) shows the broadening of the optimal band gap between 1.1-1.4 eV.

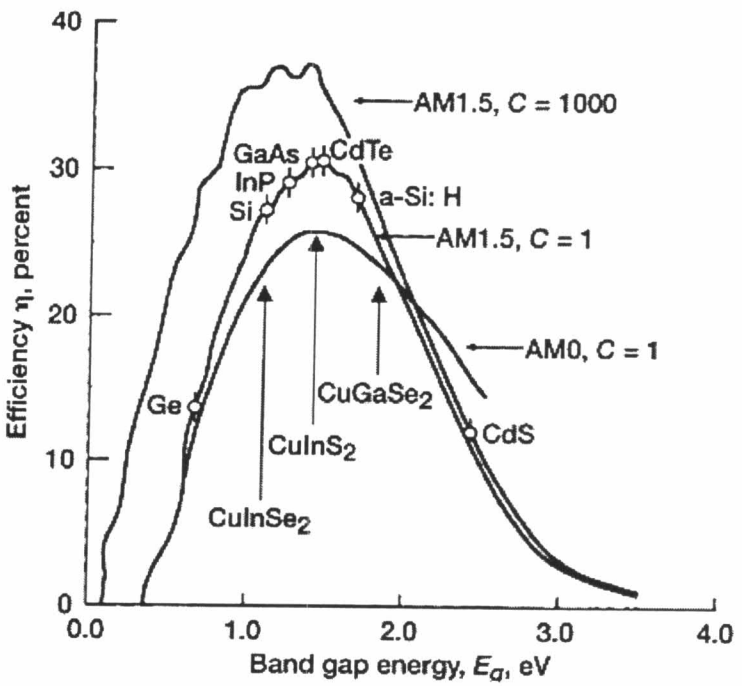

Figure 2.5: Ideal solar cell efficiency as a function of the band gap energy for the spectral distribution AM0 and AM1.5 with a power density of 1 sun, and for AM1.5 with 1000 suns (= 844 kW/m^2) [31].

2.2.2 Electrical Properties of Solar Cells

A simple band diagram for a p-n junction solar cell under illumination is shown in Fig. 2.6. In general, photons with an energy equal to or greater than the band gap are absorbed and electron–hole pairs are then created. On the other hand, photons with energy less than the band gap pass through the material and do not contribute to photovoltaic energy conversion.

Most of the electron-hole pairs are generated by light absorption and are transported by diffusion to a junction, either a p-n junction or some other types of junction, where a strong internal electric field exists. Electrons and holes are separated by the field and give rise to electric voltage and current in the external circuit, whereas the partial electron-hole pairs are lost by recombination.

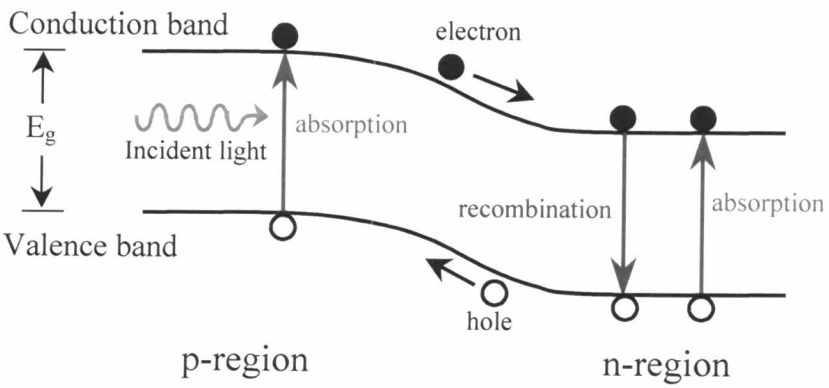

Figure 2.6: Band diagram of a p-n junction solar cell under illumination.

The current-voltage (I-V) characteristic of a solar cell can be considered by starting in the dark mode. If an external voltage is applied to the junction, the I-V characteristic can be described by the analytical solution found for Shockley-diode equation [32].

$$I = I_0\left[exp\left(\frac{qV}{AkT}\right) - 1\right] \quad , \qquad (2.3)$$

where I is the diode current flowing through device,

I_0 is the leakage current,

q is the electrical charge,

V is the bias voltage,

A is the diode quality factor,

k is Boltzmann's constant,

and T is the temperature of device.

Consider a p-n junction at zero bias under illumination, electron-hole pairs are generated. The electrons are swept to the n-side, and the holes are swept to the p-side. Therefore, the short-circuited device under illumination generates a current, and this is the light generated current or photocurrent (I_L). Since this is a drift current, its direction opposes the forward bias diffusion current (I_D) for a diode in dark thereby causing an additional current superimposed onto the diode current. Thus, under illumination, the Shockley-diode equation becomes:

$$I = I_D - I_L = I_0\left[exp\left(\frac{qV}{AkT}\right) - 1\right] - I_L \quad , \qquad (2.4)$$

where I is total current,

I_L is the photocurrent at zero bias,

and I_D is the forward bias diffusion current.

The equivalent circuit for the single junction solar cell is shown in Fig. 2.7(a). It consists of a current generator in parallel with a diode and shunt resistor leading through a series resistor to the output terminals.

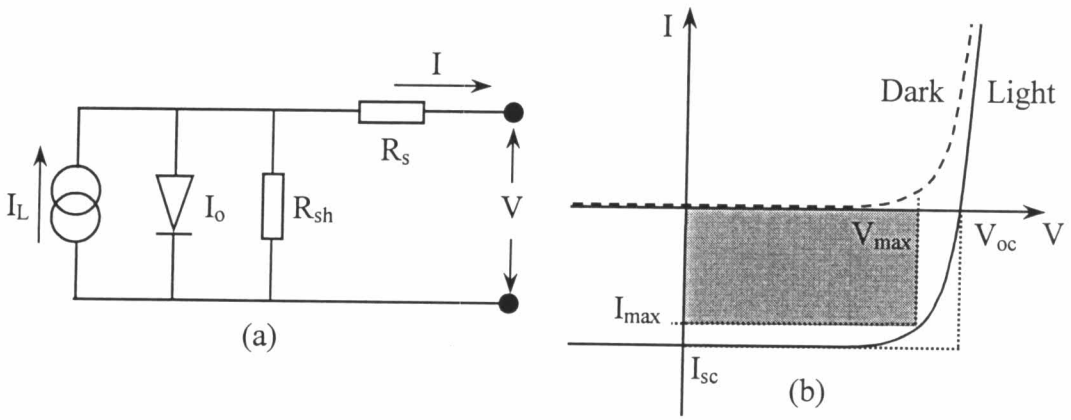

Figure 2.7: (a) The equivalent circuit of solar cells, (b) I-V characteristic curve of a solar cell in dark and under illumination. The grey rectangle defines the point of maximum output power P_{max} which is important for solar cell operation.

The series (R_S) and shunt (R_{sh}) resistances are defined as the following:

$$R_S = \left(\frac{\partial V}{\partial I} \right)\Big|_{V=V_{oc}} \quad , \qquad (2.5)$$

$$R_{sh} = \left(\frac{\partial V}{\partial I} \right)\Big|_{V=0} \quad . \qquad (2.6)$$

The R_S contribution is typically thought to manifest from resistance in the device other than the main junction, since the diode curve near V_{oc} is expected to have a small slope for an ideal diode. The R_{sh} contribution is typically thought to manifest from the main diode. This value is expected to be

large in high quality diodes. However, degradation of the main diode can result in a lowering of R_{sh} due to tunneling pathways, and shunts.

The parameters used to describe device behavior and quality are the short-circuit current (I_{sc}), the open-circuit voltage (V_{oc}), the maximum power, the fill factor (FF), the series resistance (R_s) and the shunt resistance (R_{sh}).

Ideally, the illuminated I-V curve is the dark diode curve shifted by the light generated current. The highest current value is obtained under short-circuit conditions, $V = 0$, as seen in Fig. 2.7(b). Therefore I_{sc} equals to I_L,

$$I_{sc} \equiv I_{(V=0)} = I_L \quad . \tag{2.7}$$

Setting the current in Eq. (2.4) to zero the V_{oc} is given by

$$V_{oc} = \frac{AkT}{q} ln\left[\frac{I_L}{I_0} + 1\right] \quad . \tag{2.8}$$

The V_{oc} is controlled by the current generation, recombination process and the junction transport mechanisms depending on A and I_0.

The fourth quadrant of the I-V curve determines the output power of the device, the point of maximum power being at (I_{max}, V_{max}). The shading area of the rectangular in Fig. 2.7(b) indicates the maximum output power. The FF is an expression of how "square" the output characteristics are

$$FF = \frac{V_{max} \cdot I_{max}}{V_{oc} \cdot I_{sc}} \quad . \tag{2.9}$$

Typical values for high quality devices are in the range of 0.7 to 0.85.

The three parameters V_{oc}, I_{sc} and FF are sufficient to calculate the conversion efficiency (η) of solar cells, which is defined as

$$\eta = \frac{V_{max} \cdot I_{max}}{P_{in}} \quad , \tag{2.10}$$

$$= \frac{V_{oc} \cdot I_{sc} \cdot FF}{P_{in}} \quad , \tag{2.11}$$

where P_{in} is the total radiation power incident on the solar cell.

A typical I-V curve of the actual CIGS thin film solar cell is shown in Fig. 2.8.

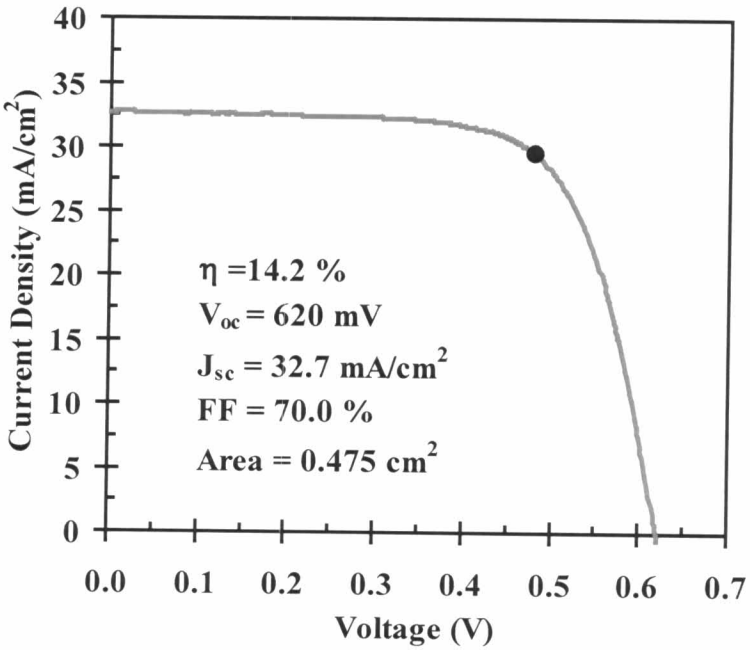

Figure 2.8: I-V curve for an actual CIGS thin film solar cell, with the solar cell parameters [33].